SAND2023-12346C

Using shockless ramp compression to investigate melting in Earth's mantle

Lindsay M. Harrison[1], Alisha N. Clark[1], Jean-Paul Davis[2], Steven D. Jacobsen[3], Adam R. Sarafian[4], and Joshua P. Townsend[2]

[1]University of Colorado, Boulder; [2]Sandia National Laboratories; [3]Northwestern University; [4]Corning, Incorporated

Motivation

Silicate melts are important agents in the formation and evolution of the Earth's crust and upper mantle. Low seismic velocity zones (LVZs) exist at regions where melts are generated, such as mid-ocean ridges and subduction zones. Some LVZs in the mantle have also been attributed to the presence of partial melts, such as at the upper and lower boundaries of the mantle transition zone (MTZ).[1,2] Melts, and their frozen counterparts, glasses, have lower seismic or sound wave speeds that distinguish them from those of crystalline material, shown in Fig. 1.[3-5] To investigate whether melts cause the MTZ-adjacent LVZs, we must understand how the density and sound velocities of amorphous silicates vary with pressure and temperature at mantle conditions.

In this work, we use pulsed-power shockless ramp compression to measure the sound velocity, longitudinal stress, and density of vitreous-SiO_2 as a melt analogue. Ramp compression is isentropic, following a pressure-temperature path more similar to the mantle geotherm than static or typical shock compression experiments, as seen in Fig. 2. We apply this new method to *v*-SiO_2. While SiO_2 is a chemically simple two-component endmember for all silicate melts, is the major constituent for natural magmas and is the basis of the aluminosilicate network which comprise the bulk of even mafic (basaltic) magmas.

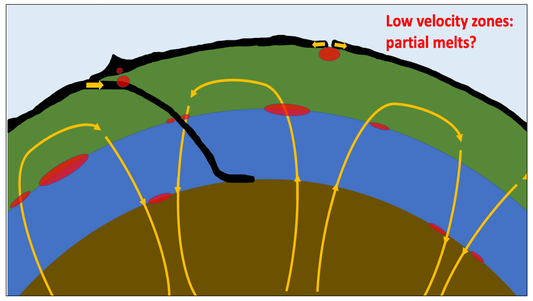

Fig. 1. A drawing of Earth's mantle with yellow arrows indicating the convective motion of material, and low velocity zones (light blue) at subduction zones and just above and below the mantle transition zone. The upper mantle, green, the transition zone, dark blue, and the lower mantle, brown. (After Hirschmann, 2006, Sakamaki, 2013 and Bercovici and Karato, 2003.)

References

1. Song, T.-R. A., Helmberger, D. V., & Grand, S. P. (2004). Nature.
2. Schmandt, B., Jacobsen, S. D., Becker, T. W., Liu, Z., & Dueker, K. G. (2014) Science.
3. Rivers, M. L., & Carmichael, I. S. E. (1987) JGR: Solid Earth.
4. Gaillard, F. (2004) Earth and Planetary Science Letters.
5. Hirschmann, M. M. (2006) Annu. Rev. of Earth and Planetary Sciences.
6. Sakamaki, T., A. Suzuki, E. Ohtani, H. Terasaki, S. Urakawa, Y. Katayama, K.-I. Funakoshi, Y. Wang, J. W. Hernlund, & M D. Ballmer. (2013) Nature Geoscience.
7. Bercovici, D., and S.-I. Karato. (2003) Nature.
8. Reisman, D. B., Stoltzfus, B. S., Stygar, W. A., Austin, K. N., Waisman, E. M., Hickman, R. J., Davis, J.-P., Haill, T. A., Knudson, M. D., Seagle, C. T., Brown, J. L., Goerz, D. A., Spielman, R. B., Goldlust, J. A., & Cravey, W. R. (2015) Physical Review Special Topics - Accelerators and Beams.
9. Davis, J.-P., Brown, J. L., Knudson, M. D., & Lemke, R. W. (2014) Journal of Applied Physics.
10. Clark, A. N. et al. (*in prep*).
11. Schroeder, J., T. G. Bilodeau, and X. S. Zhao (1990) High Pressure Research.
12. Meade, C., & Jeanloz, R. (1987) Physical Review B.
13. Petitgirard, S., Malfait, W. J., Journaux, B., Collings, I. E., Jennings, E. S., Blanchard, I., Kantor, I., Kurnosov, A., Cotte, M., Dane, T., Burghammer, M., & Rubie, D. C. (2017) Physical Review Letters.
14. Marsh, S. P. LASL Shock Hugoniot Data (University of California Press, Berkeley, 1980).
15. Zha, C.-S., R. J. Hemley, H.-K. Mao, T. S. Duffy, and C. Meade. (1994) Physical Review B.
16. Polian, A., & Grimsditch, M. (1993). Physical Review B.
17. Weigel, C., Mebarki, M., Clement, S., Vacher, R., Foret, M., and Ruffle, B. (2019) Physical Review B.
18. Sakamaki, T., Kono, Y., Wang, Y., Park, C., Yu, T., Jing, Z., & Shen, G. (2014) Earth and Planetary Science Letters.
19. Clark, A. N., Lesher, C. E., Jacobsen, S. D., & Wang, Y. (2016). JGR: Solid Earth.
20. Sanchez-Valle, C., & Bass, J. D. (2010). Earth and Planetary Science Letters.

Acknowledgments

Sandia National Laboratories is a multimission laboratory managed and operated by National Technology & Engineering Solutions of Sandia, LLC, a wholly owned subsidiary of Honeywell International Inc., for the U.S. Department of Energy's National Nuclear Security Administration under contract DE-NA0003525.

Samples provided by Corning, Incorporated.

This work is supported by the National Science Foundation under Grant EAR-1952641.

Travel expenses and conference registration is supported by the Dr. Penny E. Patterson Scholarship benefitting students at the University of Colorado Boulder Department of Geological Sciences.

Methods

- Pulsed-power machine Thor-64 shorts electric current to generate magnetic pressure waves to compress samples.[11]
- SiO_2 glass samples were compressed from 0 to 10 GPa using 10 mm-wide stripline experiment geometry.
- VISAR and PDV use 532 nm and 1550 nm coherent laser light to measure movement of the sample-window interface.

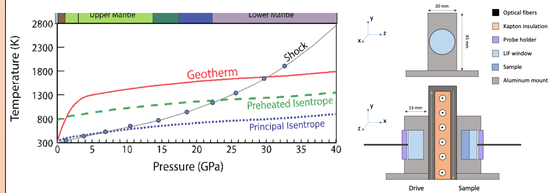

Fig. 2. Above, a photo of the magnetically-driven pulsed power machine Thor, at the Dynamic Integrated Compression Experimental (DICE) facility at Sandia National Laboratories. The sample is mounted in the center of the circular central power flow section. Below left, graph showing different experimental P-T paths with the geotherm for comparison. Below right, sample mount schematic: one side consists of a LiF window mounted directly onto the aluminum panel, and the other side consists of a SiO_2 glass sample mounted onto the aluminum panel. Current flows along the direction of the yellow arrows.

- Electrical current is stored in groups of capacitors called bricks; bricks are connected to the central power flow section by 30 m cables.

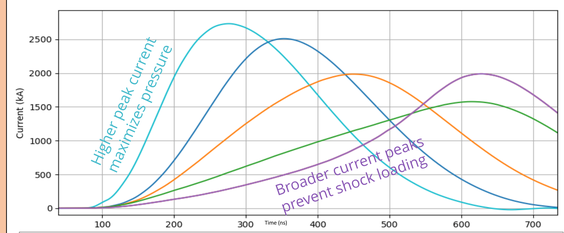

Fig. 3. Examples of pulse shapes: offsets of trigger timings control distribution of current over time. The application of current over a span of time changes the peak current of each shot. Peak current, sample material, and stripline width control peak pressures of the experiment. Each shot is uniquely tailored to achieve desired experimental pressures without shocking the sample.

Calculating sound velocities from experimental output

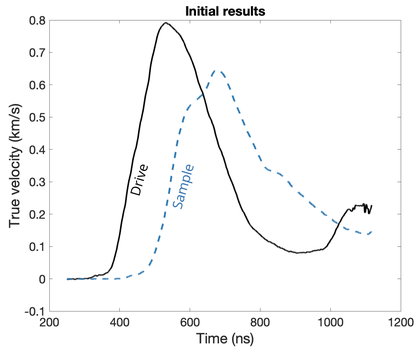

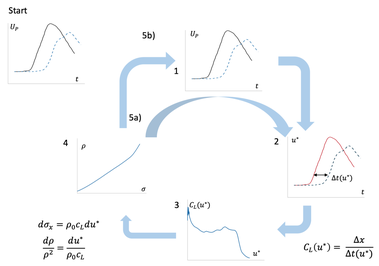

Fig. 4. Above, initial results showing surface velocities that have been corrected from noise and refractive index effects. Below, a flowchart describing the process of inverse Lagrangian analysis, the method we use to calculate the in-material sound velocity, longitudinal stress, and density from the initial results.

Results

- Sound waves in this experiment are P-waves until 0.6 km/s compression velocity; above 0.6 km/s the waves drop to bulk waves.
- Sound velocities remain relatively unchanged from 0.2 km/s through 0.6 km/s compression velocity.

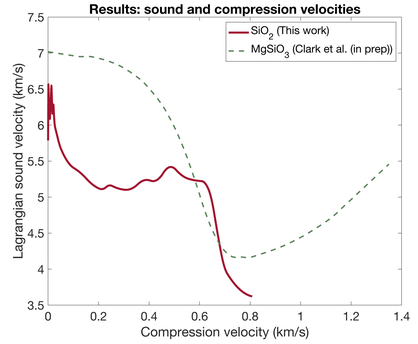

Fig. 5. Results of two ramp compression experiments on SiO_2 and $MgSiO_3$ glasses.[13] A drop in Lagrangian sound velocities for both experiments occurs at about 0.8 km/s compression velocity. These experiments had the same pulse shape yet experienced different peak stresses (see Fig. 6).

Discussion

- A transition from elastic to plastic behavior occurs at 9 GPa.
- With increasing pressure, our results show weaker pressure-dependence for density compared to static compression experiments.
- Agreement between our results and other datasets indicates that experiment timescales in dynamic compression experiments are sufficiently long and produce data that is readily applicable to the Earth.

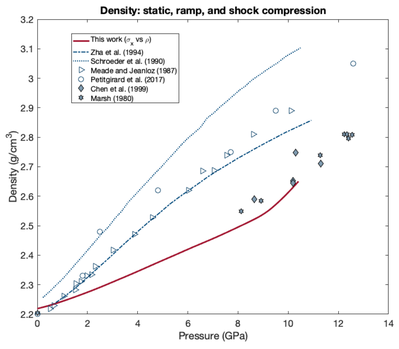

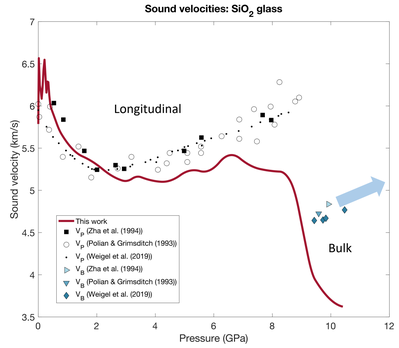

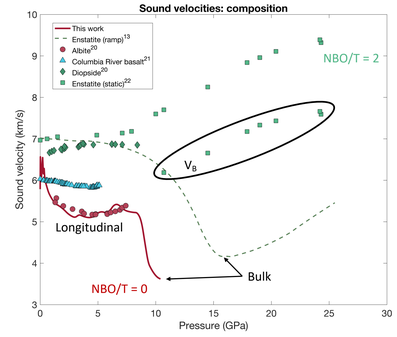

Fig. 6. Top: A comparison of density versus pressure across static, ramp, and shock compression datasets (see refs. 11, 13-16). Middle: sound speeds from this work and static compression experiments (see refs. 17-19). Longitudinal and bulk denote the types of sound velocities compared on this plot. Bottom: sound velocities across glasses of different compositions.